

## Enrichment of manganese to spessartine saturation in granite-pegmatite systems

JAMES L. MANER IV<sup>1,\*</sup>, DAVID LONDON<sup>2</sup>, AND JONATHAN P. ICENHOWER<sup>3</sup>

<sup>1</sup>Jackson School of Geosciences, Department of Geological Sciences, University of Texas at Austin, 2275 Speedway, Stop C9000, Austin, Texas 78712, U.S.A.

<sup>2</sup>ConocoPhillips School of Geology and Geophysics, University of Oklahoma, 100 East Boyd St., Room 710, Norman, Oklahoma 73019, U.S.A.

<sup>3</sup>Corning Incorporated, 21 Lynn Morse Drive, Painted Post, New York 14870, U.S.A.

### ABSTRACT

The enrichment of manganese in peraluminous (S-type) granitic melts beginning with the anatexis of metapelitic rock and ending with the crystallization of highly evolved pegmatites is explained using experimentally derived mineral-melt partition coefficients and solubility data for Mn-rich garnet. Mineral-melt partition coefficients for Fe, Mg, and Mn between garnet, cordierite, tourmaline, and peraluminous, B-bearing hydrous granitic melt were measured between 650 and 850 °C at 200 MPa<sub>H<sub>2</sub>O</sub>. The compositions of garnet and tourmaline synthesized in these experiments are similar to those found in nature. Garnets evolve from  $\text{Sps}_{51}\text{Alm}_{23}\text{Prp}_{25}$  to  $\text{Sps}_{81}\text{Alm}_{15}\text{Prp}_4$  with decreasing temperature. The Mn content of cordierite increases with decreasing temperature. The composition of tourmaline does not vary with temperature. Partition coefficients,  $D_M^{g/L}$ , and exchange coefficients,  $K_N^{g/L} = D_M^{g/L}/D_N^{g/L}$  where  $\alpha$  is a mineral,  $L$  is liquid (melt), and  $M$  and  $N$  are different elements, are presented for mineral-glass pairs. Partition coefficients for Mg, Fe, and Mn increase with decreasing temperature for garnet, tourmaline, and cordierite. The precipitation of garnet alone results in a progressive increase of MgO/FeO and a decrease of MnO/FeO in the melt. Crystallization of cordierite and tourmaline results in a decrease of MgO/FeO and an increase of MnO/FeO in melt. Tourmaline is most efficient at concentrating Mn in residual liquids. The trend toward increasing Mn/Fe in natural garnets in granites and pegmatites is not controlled by garnet itself, but instead by the crystallization of other mafic minerals in which Mg and Fe are more compatible than is Mn.

A Rayleigh fractionation model constitutes a test of the partition coefficients reported in this manuscript. The starting composition for the model is that of a liquid (melt inclusions) from an anatectic S-type source. Normative modes of cordierite and biotite are calculated from that composition and are similar to modes of these minerals in natural occurrences. The model consists of crystallization of a cordierite-biotite granite from 850 to 650 °C. The model predicts that ~95% crystallization of the starting composition is required to reach saturation in spessartine-rich garnet at near-solidus temperatures. The model, therefore, is consistent with the occurrence of spessartine as restricted to highly fractionated granite-pegmatite systems at the end stages of magmatism.

**Keywords:** Fractional crystallization, manganese, partition coefficients, tourmaline, garnet, cordierite

### INTRODUCTION

Garnet that is rich in spessartine (Sps) component,  $\text{Mn}_3\text{Al}_2\text{Si}_3\text{O}_{12}$ , occurs principally in three geologic environments. One is in cotectics, which are products of metamorphism of Mn-rich oxide nodules within aluminous marine sediment (Romer et al. 2011). A second setting is as euhedral crystals within lithophysae formed in lava flows of F-rich rhyolites, and in their analogous miarolitic granites (Christiansen et al. 1984). The third and far more common occurrence is in association with highly fractionated peraluminous granites and pegmatites, those that are characterized as S-type (Chappell and White 2001). The study presented here applies mostly to the third environment.

Melt generated by the anatexis of metasedimentary rocks, the source material of peraluminous S-type granites, contains minor to trace concentrations of the mafic elements Fe, Mg, and Mn (e.g., Acosta-Vigil et al. 2007). However, the end stages of

crystallization of S-type granitic magmas culminate in pegmatites that commonly contain spessartine-rich garnet and several phosphates near their Mn end-member compositions. Černý et al. (1985) showed that the Fe/Mn ratio of garnet decreases and the Mn content of garnet increases with the progress of crystallization from parental granites to the most evolved types of granitic pegmatites. Similarly, Miller and Stoddard (1981) observed an increase in the Mn content of garnet from the least fractionated biotite-granite to pegmatitic, garnet-muscovite granite. The evolutionary trend in garnet (Miller and Stoddard 1981; Černý et al. 1985) could be construed to signify that Fe is more compatible in garnet than is Mn, such that the eventual crystallization of spessartine results mostly from the depletion of Fe in melt through the crystallization of garnet. Experiments that entailed the crystallization of garnet from the silicic melt at the moderate pressure and temperature (650–750 °C, 200 MPa) of the cordierite-aluminum silicate facies demonstrated that Mn is more compatible than Fe in garnet at these conditions (Icenhower 1995). Therefore, other mafic phases (biotite, cordierite, and

\* E-mail: jlmaner87@gmail.com

tourmaline) in which Mn is less compatible than Fe apparently control the fractionation patterns for garnet in granitic igneous rocks (London et al. 2001). The experimental study presented here serves as a test of that hypothesis.

### PRIOR EXPERIMENTATION

The exchange of Fe and Mg between biotite and garnet (Holdaway 2004, and references therein) and between garnet and cordierite (Dwivedi et al. 1998, and references therein) have been thoroughly investigated. Van Hinsberg and Schumacher (2009) attempted to calibrate the distribution of Fe and Mg between tourmaline and biotite at hydrothermal conditions, but their experimental results showed almost no correlation between Fe-Mg exchange and temperature. Most prior studies entailed hydrothermal synthesis, and a melt was not present. Maner et al. (2013) attempted to calibrate the exchange of Fe and Mn between garnet and tourmaline as a potential geothermometer for peraluminous granitic pegmatites. Like van Hinsberg and Schumacher (2009), Maner et al. (2013) documented a wide spread in the partition coefficients and a poor correlation of element exchange with temperature. The distribution of mafic components between tourmaline and other mafic minerals and melt are unknown.

The compatibility of Mn in garnet, tourmaline, and cordierite, and the partition coefficients for Mn between these minerals and melt, are essentially unstudied through experimentation. Although mineral-melt partition coefficients for Fe and Mg might be extracted from a few experimental investigations in which mafic minerals large enough for analysis grew from the melt that is not true for Mn. Because of low Mn concentrations in typical starting materials, the concentrations of Mn in most experimental products are at or below detection levels by electron microprobe analysis.

### GOALS OF THIS RESEARCH

Although progress has been made toward understanding the mechanisms that control the compositions of garnet crystals in granitic igneous rocks, the partition coefficients for Mn among garnet, tourmaline, cordierite, and hydrous peraluminous granitic melt have not been accurately measured. These data are necessary for chemical modeling (e.g., via Rayleigh fractionation) of the Mn contents of granitic liquids. Toward this end, the primary goals of this study are to present mineral-melt partition coefficients for Mn, Fe, and Mg between hydrous peraluminous granitic melt and garnet, tourmaline, and cordierite, such as to account for the occurrence of Sps-rich garnet in the last stages of granite magmatism. Other experimental data ( $D_M^{Bt-melt}$ ; Icenhower and London 1995) are included as needed for Rayleigh modeling. The Rayleigh model serves as a test of the validity of the experimental data for the accumulation of Mn from anatexis to crystallization of cordierite- and biotite-bearing granites. Starting with an appropriate liquid composition and mineral modes, the model should, and does, predict spessartine saturation only after extended crystallization of the initial melt at near-minimum temperatures.

## METHODS

### Experimental design

Experiments were designed to crystallize garnet, cordierite, and tourmaline from nearly crystal-free hydrous, boron-bearing, peraluminous granitic melt. Some experiments were heated to 800 or 850 °C and quenched to check for crystallinity

and chemical homogeneity of the resultant liquid (quenched to glass) (Fig. 1a). Experiments intended to produce crystalline phases were either (1) quenched to room temperature from 800 or 850 °C then heated directly to the temperature of interest, (2) heated directly to a temperature between 650 and 750 °C, or (3) dropped down from 800 or 850 °C in a single isobaric cooling step to a synthesis temperature. The former experiments (1 and 2) are referred to as forward-direction experiments and the latter (3) as reverse-direction experiments<sup>1</sup>.

Several experiments conducted at 650, 700, and 750 °C had run durations between 0 and 30 days, forming a time-series for these temperatures. Zero-day experiments were quenched immediately after reaching the synthesis temperature. The composition of glass produced in these experiments was monitored for changes over time. Partition coefficients were determined using the compositions of crystal rims and adjacent liquid (glass) from all experiments, both forward and reverse thermal direction.

### Bulk compositions used in experiments

The experimental study of Wolf and London (1997) provided the starting point for our experiments. Wolf and London (1997) showed that the stability of tourmaline in granitic melt is a function of the B content and the aluminum saturation index (ASI) of melt, calculated as molar Al/(Na+K+2Ca), such that at 750 °C, tourmaline will crystallize in granitic melts having an ASI of at least 1.2 and B<sub>2</sub>O<sub>3</sub> contents above 2 wt% oxide. The ASI of each starting mixture used in the present study was controlled by adding aluminous minerals or aluminum oxide/hydroxide chemical reagents to starting material mixtures to achieve a value of at least 1.2. Boron was added to all starting material mixtures as B<sub>2</sub>O<sub>3</sub> glass, made by dehydrating boric acid in a Pt dish over a Bunsen burner. Two bulk compositions were used in this study. One bulk composition (GT1.3) contained ~3 wt% B<sub>2</sub>O<sub>3</sub> and the other (MnGT-BC-4.1) contained ~8 wt% B<sub>2</sub>O<sub>3</sub>. The elevated boron content was intended to promote crystallization of tourmaline crystals large enough for microanalysis.

The minimum concentrations of mafic oxide components in glass (melt) necessary to promote the growth of tourmaline were reported by Wolf and London (1997), and those values served as a baseline for this study. The sources of Fe, Mn, and Mg in each starting material mixture are as follows: mixture GT1.3 contained rhodonite (source of Mn), Mn-fayalite (source of Fe and Mn), and forsterite (source of Mg), and mixture MnGT-BC-4.1 contained almandine (source of Fe and Mg) and spessartine (source of Mn) (see Supplemental<sup>2</sup> Material B for details of preparation of starting materials). All starting material mixtures contained more than 1 wt% MnO to facilitate the growth of Mn-rich garnet (Icenhower 1995). Enough water was added to each capsule to ensure saturation of water in melt. No more than 15 wt% water was added to any experiment/capsule. The compositions of starting material minerals and the proportions of minerals and chemical reagents in each bulk composition are provided in Supplemental<sup>1</sup> Tables S1 and S2, respectively, in Supplemental<sup>2</sup> Material A. The composition of each glass formed by melting each starting material mixture is reported in Table 1.

### Experimental procedures

Each experiment began by adding deionized and ultra-filtered water (DIUF; Fisher Scientific) to a gold capsule of 20 × 3 mm and a wall thickness of 0.2 mm, followed by 50 to 100 mg of a starting material mixture. Loaded capsules were wrapped with a sleeve of damp paper, frozen using cryogenic spray to reduce volatilization of water during welding and sealed by Tungsten-Inert Gas (TIG; argon) welding. The capsule was then weighed to check for loss of water during welding, labeled with the appropriate experiment number, reweighed, placed in an oven at ~120 °C for at least 1 h, and then reweighed again to check for leaks in the capsule (detected as water loss by weight loss). Only capsules showing no leakage after sealing were utilized.

Experiments were conducted open to a 2 L pressure buffer in NIMONIC 105 or UDIMET cold-seal pressure vessels with water (plus a trace of Immunal as a rust inhibitor) as the pressure medium. The cool end of each vessel was tilted ~5° below horizontal to prevent the convection of water within the vessel. Hastelloy-C filler-rods, which surround the thermocouple, also reduced convection of water and heat. Temperature was monitored with an internal Chromel-Alumel thermocouple, and pressure was monitored with a factory-calibrated Heise bourdon tube gauge. Uncertainties in temperature and pressure are <10 °C and <10 MPa, respectively.

Isobaric quenching was performed by removing the vessel from the furnace and applying a jet of compressed air. The average rate of cooling is approximately 200–300 °C/min; vessels were cooled to below 150 °C before de-pressurization. Once the vessel was cool enough to handle, capsules were removed, rinsed with water, dried, weighed to check for leaks produced in the capsule during the experi-

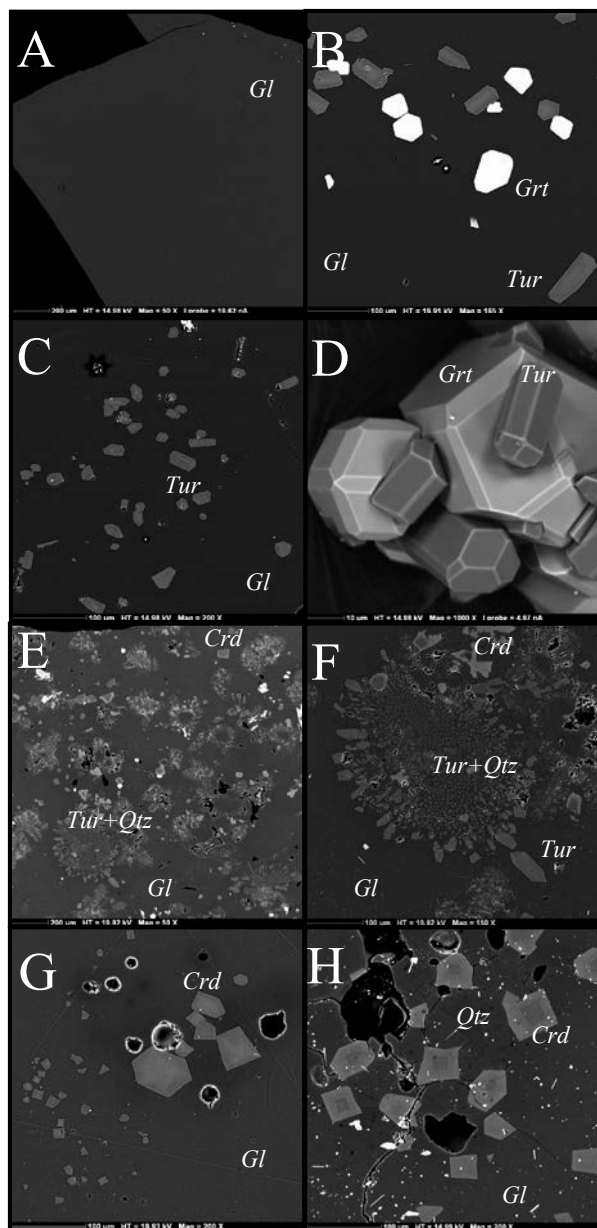


**FIGURE 1.** Backscattered electron images (BSEI) of experimental run products. Grt = garnet, Tur = tourmaline, Crd = cordierite, Qtz = quartz, Gl = glass. (a) Glass run product (Expt. no.: MnGT-80, 850 °C). (b) Euhedral garnet and tourmaline (Expt. no.: MnGT-49, “forward” to 700 °C). (c) Euhedral tourmaline crystals (Expt. no.: MnGT-56, “reverse” to 700 °C). (d) Euhedral garnet and tourmaline crystals dissolved out of glass using hydrofluoric acid (Expt. no.: MnGT-56). (e and f) Individual, euhedral cordierite crystals and clusters of cordierite, tourmaline, and quartz (Expt. no.: GBT-103, “forward” to 650 °C). (g) Cordierite (Expt. no.: GBT-90, 850 °C). (h) Intergrowth of quartz and cordierite (Expt. no.: GBT-102, “forward” to 700 °C).

ment, punctured to check for free water or volatiles, and then opened to examine the products. All experiments contained free water after quenching.

### Fugacity of oxygen in experiments

The oxygen fugacity,  $f_{O_2}$ , of the experimental system is buffered by a reaction between the water pressure medium and the Ni-based vessel and filler rod alloys.

**TABLE 1.** EMPA of starting liquid (glass) compositions

System	GT1.3		MnGT-BC-4.1	
Expt no.	GBT86		MnGT80	
T (°C)	850		850	
t (h)	24		168	
<b>Weight percent oxides</b>				
SiO <sub>2</sub>	68.47	(1.17)	62.73	(0.78)
B <sub>2</sub> O <sub>3</sub>	3.09	(0.34)	8.13	(0.44)
Al <sub>2</sub> O <sub>3</sub>	11.18	(0.36)	11.68	(0.15)
FeO*	1.39	(0.09)	0.89	(0.04)
MnO	1.52	(0.11)	1.86	(0.07)
MgO	1.00	(0.07)	0.43	(0.01)
CaO	0.22	(0.05)	0.07	(0.03)
Na <sub>2</sub> O	1.83	(0.08)	2.80	(0.11)
K <sub>2</sub> O	3.01	(0.11)	3.32	(0.11)
Total	91.70	(0.58)	91.92	(0.62)
H <sub>2</sub> O	8.30	(0.58)	8.08	(0.62)
N	25		50	
ASI	1.683	(0.070)	1.403	(0.041)
K#	0.520	(0.014)	0.439	(0.013)
Mn*	52.531	(0.828)	53.138	(0.872)
Mg#	0.561	(0.009)	0.217	(0.003)
<b>CIPW Normative mineralogy</b>				
Qz	47.32		30.63	
Or	20.05		19.62	
Ab	17.44		23.69	
An	1.21		0.35	
Crn	5.11		3.35	
Hy	8.88		6.16	

Notes: Mineral symbols after Whitney and Evans (2010). 2oSD in parentheses. ASI = aluminum saturation index [molar: Al/(Na+K)]. K# = molar K/(K+Na). Mn\* = molar Mn/(Mn+Fe)·100. Mg# = molar Mg/(Mg+Fe).

The  $f_{O_2}$  of the experimental apparatus is half a log unit below the Ni-NiO oxygen buffer (NNO) (Wolf et al. 1994) as determined from the solubility of cassiterite in reference to values cited by Taylor and Wall (1992). At this  $f_{O_2}$ , the fraction of Fe<sup>3+</sup>/Fe<sup>2+</sup> is less than 10%, based on the work of Moore et al. (1995) and Baker and Rutherford (1996) for metaluminous granitic melts at NNO and temperatures below 900 °C. The fugacity of oxygen at the NNO oxygen buffer is below that of the Mn<sub>1-x</sub>O/Mn<sub>2</sub>O<sub>3</sub> oxygen buffer (Huebner and Sato 1970); therefore, all Mn should carry a 2+ charge.

### Preparation of experimental products for analysis

Experimental products were initially examined by using a stereoscopic binocular zoom microscope and oil- or epoxy-immersed grain mounts using a transmitted light petrographic microscope. Products were prepared for qualitative and quantitative electron microprobe analysis (EMPA) by placing products in 1" circular molds or ½" brass holders and impregnated with EpoThin epoxy (Buehler). Epoxy mounts were progressively ground down with lapping films to a 3 µm grit size and then polished using diamond in water to a final grit size of ≤¼ µm. Polished experimental products were rinsed with alcohol, dried in a jet of air, and then placed in a desiccator prior to application of a carbon coat.

### Electron beam analytical methodology

Most of the imaging and analyses were performed with a CAMECA SX50 electron microprobe at the University of Oklahoma. This instrument was equipped with five wavelength-dispersive spectrometers, a PGT Prism 2000 Energy-Dispersive X-ray Analyzer (EDXA) with Moxtek polymer entry window, and PC-based SAMx automation system for both analysis and imaging. A small number of analyses were performed using a CAMECA SX100 microprobe beginning in 2015. Qualitative phase identification was accomplished using backscattered electron imaging coupled with EDXA using either a 15 or 20 kV accelerating voltage and 20 nA beam current.

Quantitative analyses were performed by wavelength-dispersive spectrometry (WDS). Analytical conditions for tourmaline, garnet, and cordierite utilized a 15 kV accelerating voltage, 20 nA beam current, and 2 µm spot. Elements analyzed in tourmaline included B, F, Na, Mg, Al, Si, Ca, Ti, Mn, and Fe. Garnet and cordierite crystals were analyzed for Fe, Mn, Na, Si, Cr, Ti, Al, Mg, K, and Ca. Glass analyses used a two-condition routine to mitigate the migration of Na during analysis (Morgan and London 1996, 2005). The first condition used 15 kV accelerating voltage, 2 nA beam current, and 20 µm spot for analysis of Na, K, Ca, Al, and Si; the second

condition used 15 kV accelerating voltage, 40 nA beam current, and 20  $\mu\text{m}$  spot for analysis of Mg, Mn, Fe, Ti, F, and B. Counting times for all elements resulted in detection limits less than 0.05 wt% oxide except for B and F, which had a detection limits of 0.24 wt% oxide and 0.20 wt% element, respectively. Data reduction employed the PAP method (Pouchou and Pichoir 1985). The average composition of all synthetic minerals and glasses are reported in Supplemental<sup>2</sup> Tables S3 through S6 in Supplemental<sup>2</sup> Material A.

### Mineral formula calculations

Chemical formulas for garnet and cordierite crystals were calculated from EMPA chemical data based on 12 and 18 oxygen atoms, respectively (see Table 2 for end-member compositions). The chemical formula of the garnet group is  $\{X_3\}[Y_2](Z_3)O_{12}$  (Grew et al. 2013). Site assignments follow the method of Grew et al. (2013) and only include elements analyzed in this study. The chemical formula of the cordierite group is  $M_2Al_4Si_6O_{18}$ , where M can be occupied by Fe, Mg, and Mn.

The chemical formula for minerals of the tourmaline supergroup is  $XY_2Z_6(BO_3)_3(T_3O_9)(V)_3(W)$  (Henry et al. 2011) (see Table 2 for pertinent end-member compositions). Cations were calculated from EMPA data on a 29-oxygen atom basis. An Excel spreadsheet developed by Morgan (2016) was used to calculate the percentages of end-member tourmaline components from the EMPA data.

**TABLE 2.** Chemical formulas of pertinent minerals

Species	Abbreviation	Chemical formula
Indialite	Ind	$Mg_2Al_4Si_6O_{18}$
Sekaniite	Sek	$Fe_2Al_4Si_6O_{18}$
Spessartine	Sps	$Mn_3Al_3Si_3O_{12}$
Almandine	Alm	$Fe_3Al_3Si_3O_{12}$
Pyrope	Prp	$Mg_3Al_3Si_3O_{12}$
Schorl	Srl	$NaFe_3Al_6(BO_3)_3Si_6O_{18}(OH)_4$
Dravite	Drv	$NaMg_3Al_6(BO_3)_3Si_6O_{18}(OH)_4$
"Tsilaisite"	Tsi	$NaMn_3Al_6(BO_3)_3Si_6O_{18}(OH)_4$
Olenite	Ol	$NaAl_3Al_6(BO_3)_3Si_6O_{18}(OH)_4$
Foiteite	Ftt <sup>a</sup>	$\square(Fe_2Al)Al_6(BO_3)_3Si_6O_{18}(OH)_4$
Magnesiofoiteite	Ftt <sup>b</sup>	$\square(Mg_2Al)Al_6(BO_3)_3Si_6O_{18}(OH)_4$
Uvite	Uv <sup>b</sup>	$CaMg_3(MgAl_3)(BO_3)_3Si_6O_{18}(OH)_4$
Feruvite	Uv <sup>b</sup>	$CaFe_3(MgAl_3)(BO_3)_3Si_6O_{18}(OH)_4$

Notes:  $\square$  = site vacancy. Most mineral symbols after Whitney and Evans (2010).  
<sup>a</sup> Foiteite and Mg-foiteite are combined into a single Foiteite component in the text.  
<sup>b</sup> Uvite and Fe-uvite are combined into a single Uvite component in the text.

## RESULTS

### Description of products: Textures and compositions

Synthetic crystalline products include tourmaline, cordierite, garnet, quartz, alkali feldspar, corundum/mullite, and Mn-Fe-Ni-Cr-Al oxides. The compositions of oxide minerals, as determined by EDS analysis, are dominantly Fe-Al-rich (hercynite), with minor to trace amounts of Ni, Cr, and Mn. The source of Ni and Cr in the experiments is the reaction vessel itself (NIMONIC Ni-Cr alloy) (Puziewicz and Johannes 1988). Most oxide and all corundum/mullite crystals are too small for accurate characterization by EPMA methods. At the pre-conditioning step (800 and 850 °C), trace quantities of relict starting materials (garnet) persisted in experiments that used bulk composition MnGT-BC-4.1. Cordierite crystallized and grains of quartz (added as a starting material) had resorbed textures in pre-conditioned experiments using bulk composition GT-1.3. Spinel and corundum/mullite crystallized in some experiments at the pre-conditioning stage.

Glass (melt) was the dominant phase in all pre-conditioned experiments using bulk composition MnGT-BC-4.1 (Fig. 1a). Garnet and tourmaline crystallized in all experiments between 750 and 650 °C using bulk composition MnGT-BC-4.1 (Figs. 1b–1d). Cordierite and garnet crystallized in all experiments using bulk composition GT-1.3. Cordierite did not crystallize in any experiment that utilized bulk composition MnGT-BC-4.1. Tourmaline crystallized with garnet and cordierite in one experiment (GBT103) at 650 °C using bulk composition GT-1.3. Forward and reverse direction experiments that started at a temperature above the liquidus produced the same crystalline assemblage. Quartz and alkali feldspar were only identified in experiments that were heated directly to the temperature of interest and held at that temperature for 720 h (Table 3: MnGT-126, GBT-103, MnGT-125).

**TABLE 3.** Conditions of experiments and summary of compositions of crystalline products

Expt. no.	T (°C)	Direction <sup>a</sup>	Time (h)	System <sup>b</sup>	Products <sup>c</sup>	Garnet			Tourmaline				Cordierite		
						Xsps	Xalm	Xprp	Xdrv	Xsrl	Xftt	Xuv	Xind	Xsek	XMn
GBT90	850	F	45	GT1.3	Grt, Crd	50.63	23.38	25.99	–	–	–	–	74.47	14.16	11.37
GBT88	750	FF	168	"	Grt, Crd	55.89	26.86	17.24	–	–	–	–	67.84	18.97	13.19
GBT89	750	F	168	"	Grt, Crd	67.17	21.93	10.89	–	–	–	–	–	–	–
GBT101	750	FF	456	"	Grt, Crd	63.20	22.80	14.00	–	–	–	–	66.25	16.36	17.39
GBT102	700	FF	336	"	Grt (trace), Crd	–	–	–	–	–	–	–	68.89	12.95	18.06
GBT103	650	FF	456	"	Grt, Tur, Crd, Qtz	81.12	14.98	3.91	36.30	24.48	17.77	14.27	48.03	21.79	30.18
MnGT111	850	F	168	MnGT-BC-4.1	–	–	–	–	–	–	–	–	–	–	–
MnGT103	750	R	0	"	–	–	–	–	–	–	–	–	–	–	–
MnGT77	750	R	24	"	Grt, Tur (trace)	72.80	15.26	11.93	39.59	25.53	30.90	0.79	–	–	–
MnGT104	750	R	24	"	–	–	–	–	–	–	–	–	–	–	–
MnGT110	750	R	168	"	–	–	–	–	–	–	–	–	–	–	–
MnGT112	750	R	336	"	–	–	–	–	–	–	–	–	–	–	–
MnGT126	750	F	720	"	Grt (relict), Tur, Qtz, AFS	–	–	–	–	–	–	–	–	–	–
MnGT65	700	R	0	"	–	–	–	–	–	–	–	–	–	–	–
MnGT66	700	R	24	"	Grt (trace), Tur	–	–	–	41.61	27.44	18.62	7.45	–	–	–
MnGT67	700	R	72	"	Grt (trace), Tur	–	–	–	40.21	27.44	20.08	7.60	–	–	–
MnGT49	700	FF	264	"	Grt, Tur	70.80	19.95	9.25	34.90	27.98	20.46	8.14	–	–	–
MnGT56	700	R	336	"	Grt, Tur	80.83	13.29	5.89	40.80	28.05	18.34	8.39	–	–	–
MnGT125	700	F	720	"	Grt (relict), Tur, Qtz	–	–	–	–	–	–	–	–	–	–
MnGT114	650	R	0	"	Bt	–	–	–	–	–	–	–	–	–	–
MnGT116	650	R	24	"	–	–	–	–	–	–	–	–	–	–	–
MnGT117	650	R	720	"	Bt	–	–	–	–	–	–	–	–	–	–
MnGT124	650	F	720	"	Grt (relict), Tur	–	–	–	–	–	–	–	–	–	–

Notes: X = mole fraction mineral end-member [spessartine (sps), almandine (alm), pyrope (prp), dravite (drv), schorl (srl), total foiteite (ftt), uvite (uv), indialite (ind), sekaniite (sek), Mn-crd (Mn)] foiteite and uvite components represent total Mg-foiteite+foiteite and feruvite+uvite, respectively.

<sup>a</sup> F (Heated directly to temperature), FF (heated to temperature above liquidus, quenched, and then heated directly to temperature of interest), R (heated to temperature above liquidus, quenched, and then cooled to temperature of interest).

<sup>b</sup> System = bulk composition (Table 1).

<sup>c</sup> Garnet (Grt), cordierite (Crd), tourmaline (Tur), quartz (Qtz), alkali-feldspar (AFS). All products include glass and trace amounts of mullite/corundum and Fe-Mn-Ni-Cr oxides.

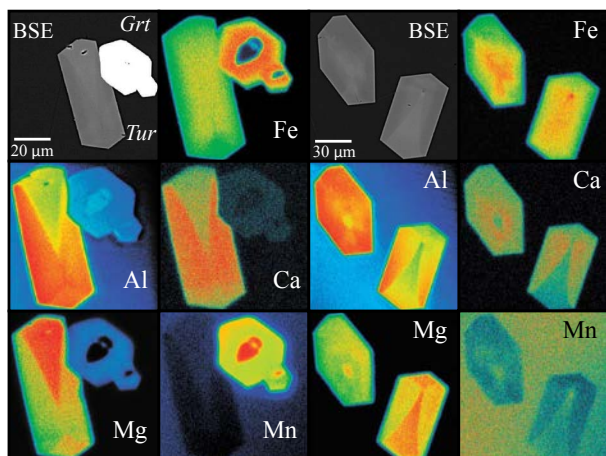


**FIGURE 2.** X-ray maps of Fe, Mn, Mg, Ca, and Al in garnet and tourmaline produced in experiment MnGT49 (700 °C, 264 h). Experiment MnGT49 was heated to 800 °C, quenched, and then heated directly 700 °C. Note the sector zoning of Al, Ca, and Mg in tourmaline. The Mn-rich cores of garnets are relict Mn-rich garnet starting material. (Color online.)

**Garnet.** Garnet crystals are a solid solution of spessartine (Sps), almandine (Alm), and pyrope (Prp) (Table 3). Garnet formed euhedral crystals that display abrupt core-rim chemical zonation in all experiments (Fig. 2). The cores of each garnet crystal are relict Mn-rich or Fe-rich garnet starting material grains. Rim compositions of all garnets reflect growth at the synthesis, low-temperature, stage of each experiment. The compositions of garnet generally follow a temperature-dependent trend from  $\text{Sps}_{51}\text{Alm}_{23}\text{Prp}_{25}$  to  $\text{Sps}_{81}\text{Alm}_{15}\text{Prp}_4$  with decreasing temperature (Table 3, Figs. 3a and 3b). A full Y-site, i.e., two Al cations, is supportive evidence of a low fraction of  $\text{Fe}^{3+}$  in the melt.

**Tourmaline.** In experiments that utilized bulk composition MnGT-BC-4.1, tourmaline formed euhedral, prismatic crystals in experiments between 750 and 700 °C, in both forward and reverse experiments (Figs. 1b–1d). Below 700 °C, tourmaline crystallized as radial clusters intergrown with quartz (Figs. 1e–1f) and as isolated skeletal (soda-straw) crystals irrespective of thermal direction. Tourmaline only crystallized at 650 °C in experiments that utilized bulk composition GT1.3.

Tourmaline crystals are dominantly a solid solution of schorl, dravite, and foitite with minor amounts of uvite (Table 3). The compositions of tourmaline do not change as a function of temperature. The average MnO content of tourmaline is ranges from ~0.7 wt% at 750 °C to ~1.5 wt% at 650 °C. Tourmaline crystals synthesized at 700 °C display weak hourglass sector-zonation; the *a* and *c*-axial sectors are Al- and Ca-rich and Mg-poor relative to the *c*<sup>+</sup> axial sector (Fig. 2) (Maner et al. 2014).

**Cordierite.** Cordierite consistently formed euhedral crystals and displays abrupt core-rim chemical zonation in all experiments below 800 °C (Figs. 1g and 1h). All cores have compositions that reflect growth at the pre-conditioning, high-temperature, stage. The rim compositions of cordierite (Crd) crystals are Mg-rich (indialite = Ind) at high temperature and, apart from a single experiment at 700 °C (GBT-102), evolve toward higher Fe (sekaninaite = Sek) and Mn compositions with decreasing temperature (Fig. 3c). Five cordierite crystals from experiment GBT-103 (650 °C, 200 MPa,

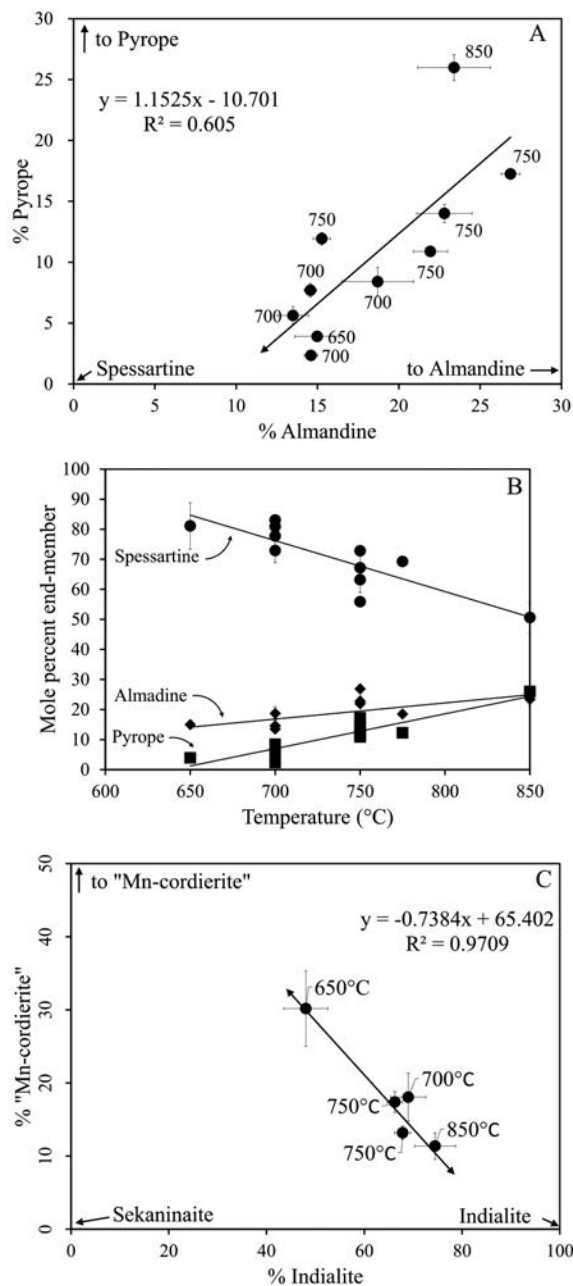


**FIGURE 3.** (a) Composition of garnet, represented as the mole percentage of almandine (alm) and pyrope (prp), produced in this study. The mole percent of spessartine can be calculated by subtracting the percent of almandine and the percent of pyrope from 100%. (b) Mole percentages of end-member garnet species (spessartine, almandine, and pyrope) plotted against temperature. Note the linear trend of decreasing Fe and Mg and increasing Mn with decreasing temperature. (c) The composition of cordierite, as molar percentages of “Mn-cordierite” and indialite (Mg-Crd), produced in experiments in this study. The mole percentage of sekaninaite (Fe-Crd) can be calculated by subtracting the percent of “Mn-cordierite” and the percent of indialite from 100%. Apart from the single experiment conducted at 700 °C, the Mn and Fe content increases with decreasing temperature. All symbols reflect the average composition of garnet or cordierite from each experiment reported in this manuscript (not from literature).

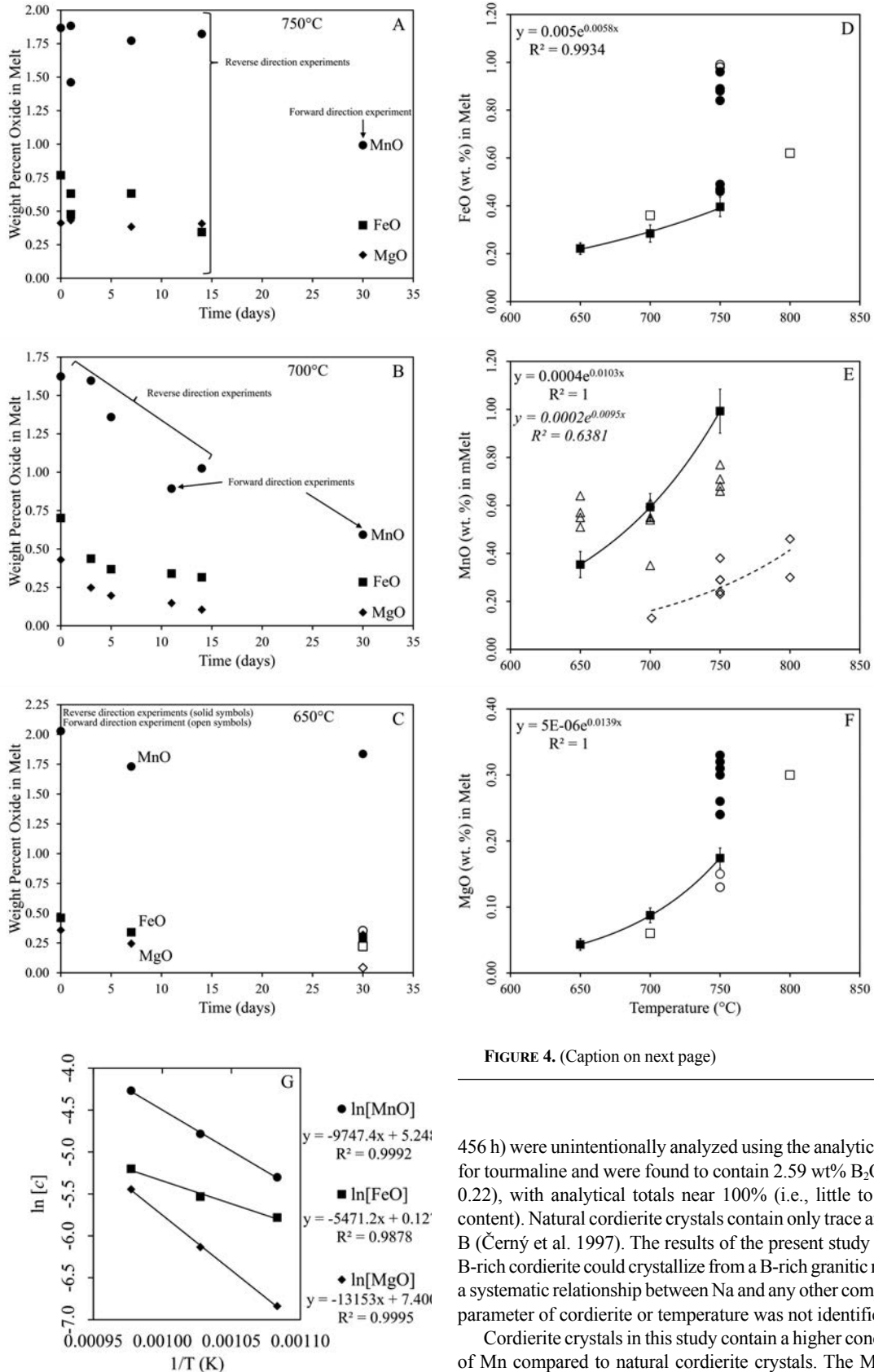


FIGURE 4. (Caption on next page)

456 h) were unintentionally analyzed using the analytical method for tourmaline and were found to contain 2.59 wt% B<sub>2</sub>O<sub>3</sub> (1σSD: 0.22), with analytical totals near 100% (i.e., little to no water content). Natural cordierite crystals contain only trace amounts of B (Černý et al. 1997). The results of the present study show that B-rich cordierite could crystallize from a B-rich granitic melt. Last, a systematic relationship between Na and any other compositional parameter of cordierite or temperature was not identified.

Cordierite crystals in this study contain a higher concentration of Mn compared to natural cordierite crystals. The Mn content

◀ **FIGURE 4.** Solubility of FeO, MgO, and MnO at garnet and tourmaline saturation. (a, b, and c) Display of a time series of experiments conducted between 0 and 720 h at 750, 700, and 650 °C, respectively. Circles, squares, and diamonds represent the concentrations of MnO, FeO, and MgO, respectively, in glass. Data shown in panels d, e, and f represent the concentrations of FeO, MnO, and MgO in glass, respectively, at garnet and tourmaline saturation. Solid squares are data presented in this manuscript from long-duration (720 h) experiments using bulk composition MnGT-BC-4.1 in which steady-state conditions have been validated via a time-series of experiments. Open circles and solid circles are data from Wolf and London (1997) for tourmaline growth and dissolution, respectively, from/into granitic melt. Open squares are from Acosta-Vigil et al. (2003) for tourmaline dissolution in granitic melt. Data from F-rich (~1 wt% F) experiments of Icenhower (1995) and from B- and F-free, hydrous (~5–7% H<sub>2</sub>O) experiments of London et al. (2012a) are shown for comparison (open diamonds). Error bars represent 2σ standard deviations. (g) Natural log of the concentrations of FeO (squares), MnO (triangles), and MgO (diamonds) in hydrous, boron-bearing granitic melt plotted against 1/T (K). The data are from long-duration (720 h) experiments. The linear nature of the data, and the high correlation coefficients ( $r^2 > 0.98$ ) for each line, confirm that the compositions presented in this study represent near-equilibrium conditions between crystal and melt.

of cordierite in this study increases with decreasing temperature from 11.37 mol% “Mn-cordierite” at 850 °C to 30.18 mol% “Mn-cordierite” at 650 °C (Fig. 3c). Jobin-Bevans and Černý (1998) noted that most natural cordierite crystals contain less than ~10 mol% of the Mn end-member. Dasgupta et al. (1974) conducted experiments in the system MnO-Al<sub>2</sub>O<sub>3</sub>-SiO<sub>2</sub>-H<sub>2</sub>O and found that “Mn-cordierite” is a stable phase below 400 °C and 100 MPa but breaks down to spessartine-aluminosilicate-quartz above this pressure and temperature. Though a natural occurrence of cordierite and Mn-rich garnet has not been reported, and the experimental study of Dasgupta et al. (1974) suggests such an assemblage could not exist, the results in the present experimental study indicate that Mn-rich cordierite can exist with Mn-rich garnet at a pressure of 200 MPa and between 650 and 750 °C.

**Glass.** Compositions of all glasses (melts) are reported in Supplemental<sup>2</sup> Material A. The composition of glass produced at 850 °C is a close approximation of the bulk composition of the system because the glasses are nearly crystal free. The bulk compositions of each system (GT1.3 and MnGT-BC-4.1) are reported in Table 1. The melt (glass) produced using bulk composition GT1.3 has a higher normative quartz component compared to bulk composition MnGT-BC-4.1, whose composition is near the thermal minimum of the water-saturated haplogranite system at 200 MPa. The sum of FeO, MnO, and MgO in glass decreases from 1.56 to 0.62 wt% from 750 to 650 °C in experiments that produced both garnet and tourmaline (bulk composition MnGT-BC-4.1). Changes in the concentrations of MnO, FeO, and MgO were monitored over time through a series of experiments conducted at one temperature but with different durations (Figs. 4a–4c). Steady-state conditions, in which the compositions of melt do not change over time, were achieved by 30 days; these conditions represent a close approach to equilibrium between melt and crystals. The results shown in Figures 4d to 4g represent the concentrations of FeO, MnO and MgO in glass from experiments with durations of 30 days. As shown in Figures 4d to 4f, the concentrations of MnO, FeO, and MgO increase exponentially with temperature. The natural log of the concentrations of MnO, FeO, and MgO in melt are plotted against 1/T (K) in Figure 4g, e.g., a van’t Hoff-style diagram. The linear trends shown in Figure 4g are supportive evidence of near-equilibrium conditions between crystals and melt. The normative corundum component of glass increases linearly with temperature (Fig. 5). The solubility data reported in this study is similar to data reported in previous studies (e.g., Icenhower 1995; Icenhower and London 1995; Wolf and London 1997; Acosta-Vigil et al. 2003), which is further supportive evidence that the values reported in all of these studies represent near-equilibrium results.

### Mineral-melt partition coefficients and exchange coefficients

Partition coefficients,  $D_M^{a/L}$ , where  $a$  is a mineral and  $L$  is melt, were calculated as the concentration in weight percent of an oxide in mineral divided by the weight percent oxide in glass (Beattie et al. 1993; Janoušek et al. 2015). Bulk partition coefficients,  $WD_M^{a/L}$ , are defined as the partition coefficient,  $D$ , multiplied by the weight fraction of the mineral (Beattie et al. 1993). Values of  $WD_M^{a/L}$  are used in the Rayleigh equation to model the compositional evolution of melt, i.e., the liquid line of descent, during fractional crystallization. Partition coefficients for MnO, FeO, and MgO between garnet- and cordierite-melt were measured in the temperature interval 650 to 850 °C and between 650 to 750 °C for tourmaline-melt (Table 4). Data for  $D^{Bt/melt}$  (Icenhower and London 1995),  $D^{Crd/melt}$  (Icenhower 1995; Wolf and London 1997; Evensen and London 2003), and  $D^{Tur/melt}$  (Wolf and London 1997; Van Hinsberg 2011) are reported in the Supplemental<sup>2</sup> Material A to complement and compare to the data measured in this study.

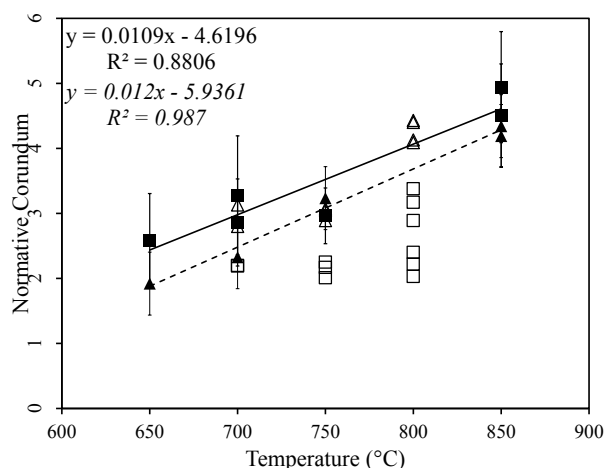


**FIGURE 5.** Normative corundum component of boron-bearing, peraluminous, hydrous granitic melts (glasses) that produced garnet and cordierite crystals (solid squares = bulk composition GT1.3) and tourmaline (solid triangle = bulk composition MnGT-BC-4.1). Data from Acosta-Vigil et al. (2003) for dissolution of cordierite (open squares) and tourmaline (open triangles) into boron-free (for cordierite) and boron-bearing (for tourmaline), hydrous granitic melt. The italicized equation and correlation coefficient belong to the dashed line. Errors for solid squares are 2σ standard deviations. Errors for open symbols are similar to the size of the symbol. Note the lower normative corundum for cordierite dissolution into B-free granitic melt compared with the data for B-bearing granitic melt.

All values of  $D_M^{w/l}$  measured in the present study increase with decreasing temperature (Figs. 6a–6f) and all partition coefficients are  $\geq 1$ , except for  $D_{MnO}^{Tur-melt}$  above 650 °C. It is for these reasons that the total mafic component of anatectic granitic melts (saturated in one or more of these mafic minerals) is  $< 2$  wt% total oxides up to 800 °C at  $f_{O_2} = NNO$  and  $< 4\%$  of normative mafic mineral components (see Supplemental<sup>2</sup> Material A), and those values decrease with crystallization toward the thermal minimum, resulting in leucogranites and pegmatites that are nearly free of mafic components, except for Mn.

Exchange coefficients, given the symbol  $K_{D(MN)}$  where M and N are different oxides (Beattie et al. 1993), compare pairs of mineral/melt partition coefficients for the same mineral (see endnote 1). Figures 7a and 7b show exchange coefficients MgO/FeO and MnO/FeO for garnet, tourmaline, biotite, and cordierite. The  $D$  values used to construct Figures 7a and 7b derive from experiments reported in this study and from the literature (Icenhower 1995; Icenhower and London 1995; Evensen and London 2003). It is also important to note that the  $D$  values were calculated from data for mineral-melt pairs from experiments conducted in the temperature range of 650 to 850 °C and 200 MPa. In Figures 7a and 7b, the slope of the line regressed through the data represents the exchange coefficient, e.g.,  $K_{D(MnO/FeO)}$ . A slope greater than one indicates that the element in the numerator will be depleted from melt faster than the element in the denominator. For example, in Figure 7b, values of  $D_{MnO}$  are greater than values of  $D_{FeO}$  for garnet, which means that crystallization of garnet will result in a decrease in the MnO/FeO ratio of residual melt.

Although  $D$  values tend to increase with decreasing temperature (Fig. 6),  $K_D$  values do not appear to vary as a function of temperature (Figs. 7a and 7b). Exchange coefficients for Fe/Mg between olivine (Roeder and Emslie 1970; Ulmer 1989) and basaltic liquid and for Ca/Na between plagioclase and basaltic liquid have been shown to be independent of temperature (Berndt et al. 2005). Berndt et al. (2005) observed that the  $K_D$  value for Fe/Mg between olivine and basaltic melt does change as a function of Fe/Mg ratio of the liquid phase. The  $K_D$  values reported here for garnet, tourmaline, and cordierite might change over a wider range of compositions. However, aside from the high concentration of  $B_2O_3$ ,

used in the experiments, the liquid compositions used in this study are similar to whole-rock compositions for many S-type granites.

## DISCUSSION

### The evolution of MgO/FeO and MnO/FeO of melt during fractional crystallization

The MgO/FeO ratio of granites decreases (Frost et al. 2001, and references therein) and MnO/FeO ratio increases (Černý et al. 1985) during the fractional crystallization of predominantly S-type granitic melts that are the sources of highly fractionated leucogranites (e.g., Pedrobernardo, Spain: Bea et al. 1994) and rare-element pegmatites (e.g., Černý et al. 1985) that contain spessartine. An increase in the MnO/FeO ratio during fractional crystallization of granites must be controlled by the crystallization of minerals in which Mn is less compatible than Fe and Mg. Similarly, the MgO/FeO ratio decreases due to the greater compatibility of Mg compared to Fe in mafic phases at high temperature.

The data plotted in Figures 7a and 7b show that crystallization of biotite and cordierite depletes the melt in MgO relative to FeO most effectively and that the crystallization of tourmaline and biotite promotes an increase in the MnO content of melt relative to FeO. Values of  $K_D^{MnO/FeO}$  decrease in the sequence from garnet to cordierite to biotite to tourmaline (Fig. 7b). Thus, the crystallization of garnet only will produce a steady decrease in the MnO/FeO ratio of melt and of garnet (e.g., Müller et al. 2012). Among all mafic phases, the MnO/FeO ratio of the melt increases most rapidly with the crystallization of tourmaline.

These trends are seen more clearly in solutions to the Rayleigh fractionation equation,

$$C = F^{D-1} \times C_0$$

where  $C$  is the concentration of an element as an oxide in melt (e.g., MnO or FeO),  $C_0$  is the initial concentration of an element as an oxide in melt,  $F$  is the fraction of liquid, and  $D$  is the mineral-melt partition coefficient. To model a ratio, e.g., MnO/FeO, the Rayleigh equation is re-arranged as

$$\frac{MnO}{FeO} = F^{(D_{MnO}^{mineral-melt} - 1) - (D_{FeO}^{mineral-melt} - 1)} \times \frac{MnO_0}{FeO_0}$$

The individual effects of biotite, garnet, cordierite, and tourmaline crystallization on the MgO/FeO and MnO/FeO ratios of melt are shown in Figures 8a and 8b, respectively. The model depicted in Figures 8a and 8b assumes crystallization of 95% quartz and feldspar and 5% mafic mineral at a temperature of 650 °C. Partition coefficients from experiments conducted at 650 °C are used in the Rayleigh equation [garnet, cordierite, and tourmaline: Expt. GBT-103, Table 4; Biotite:  $D_{Bi-melt}^{MnO} = 5.4$ ,  $D_{Bi-melt}^{FeO} = 24.7$ ,  $D_{Bi-melt}^{MgO} = 58.5$ , average of five experiments from Icenhower and London (1995)]. The partition coefficients presented in this study have been shown to increase with decreasing temperature. Therefore, the results of the Rayleigh model, which assumes crystallization at 650 °C, represents one condition. The use of partition coefficients from higher temperature experiments would result in a smaller change in the MnO/FeO ratio during fractional crystallization. The partition coefficients for quartz and feldspar are set to zero. Bulk partition coefficients are calculated using experimentally measured partition coefficients for garnet and tourmaline (experi-

TABLE 4. Mineral-melt partition coefficients

	Expt. no.	BC	T (°C)	$D_{FeO}$	$D_{MnO}$	$D_{MgO}$	
Grt/melt	GBT-90	1.3	850	8.07	15.62	7.45	w/Crd
Grt/melt	GBT-88	1.3	750	11.82	20.74	8.74	w/Crd
Grt/melt	GBT-101	1.3	750	21.56	24.85	8.91	w/Crd
Grt/melt	GBT-89	1.3	750	14.91	44.96	11.93	w/Crd
Grt/melt	MnGT-77	4.1	750	11.31	23.01	7.23	w/Tur
Grt/melt	MnGT-49	4.1	700	26.78	35.69	16.01	w/Tur
Grt/melt	MnGT-56	4.1	700	19.95	36.37	14.02	w/Tur
Grt/melt	GBT-103	1.3	650	22.53	38.76	7.93	w/Crd&Tur
Crd/melt	GBT-90	1.3	850	2.55	1.83	11.14	w/Grt
Crd/melt	GBT-88	1.3	750	4.39	2.57	18.07	w/Grt
Crd/melt	GBT-101	1.3	750	8.01	3.54	21.84	w/Grt
Crd/melt	GBT-102	1.3	700	6.79	3.64	31.95	w/Grt
Crd/melt	GBT-103	1.3	650	16.73	7.37	49.77	w/Grt&Tur
Tur/melt	MnGT-77	4.1	750	14.64	0.46	14.11	w/Grt
Tur/melt	MnGT-49	4.1	700	23.52	0.64	37.88	w/Grt
Tur/melt	MnGT-56	4.1	700	31.11	0.90	–	w/Grt
Tur/melt	MnGT-66	4.1	700	20.89	0.64	26.14	Tur only
Tur/melt	MnGT-67	4.1	700	25.42	0.72	33.02	Tur only
Tur/melt	GBT-103	1.3	650	30.28	1.62	49.93	w/Grt&Crd

Notes: BC = bulk composition. Tourmaline (Tur), garnet (Grt), cordierite (Crd). Errors for mean  $D$  values are less than 10% relative, and most commonly  $\sim 5\%$ .

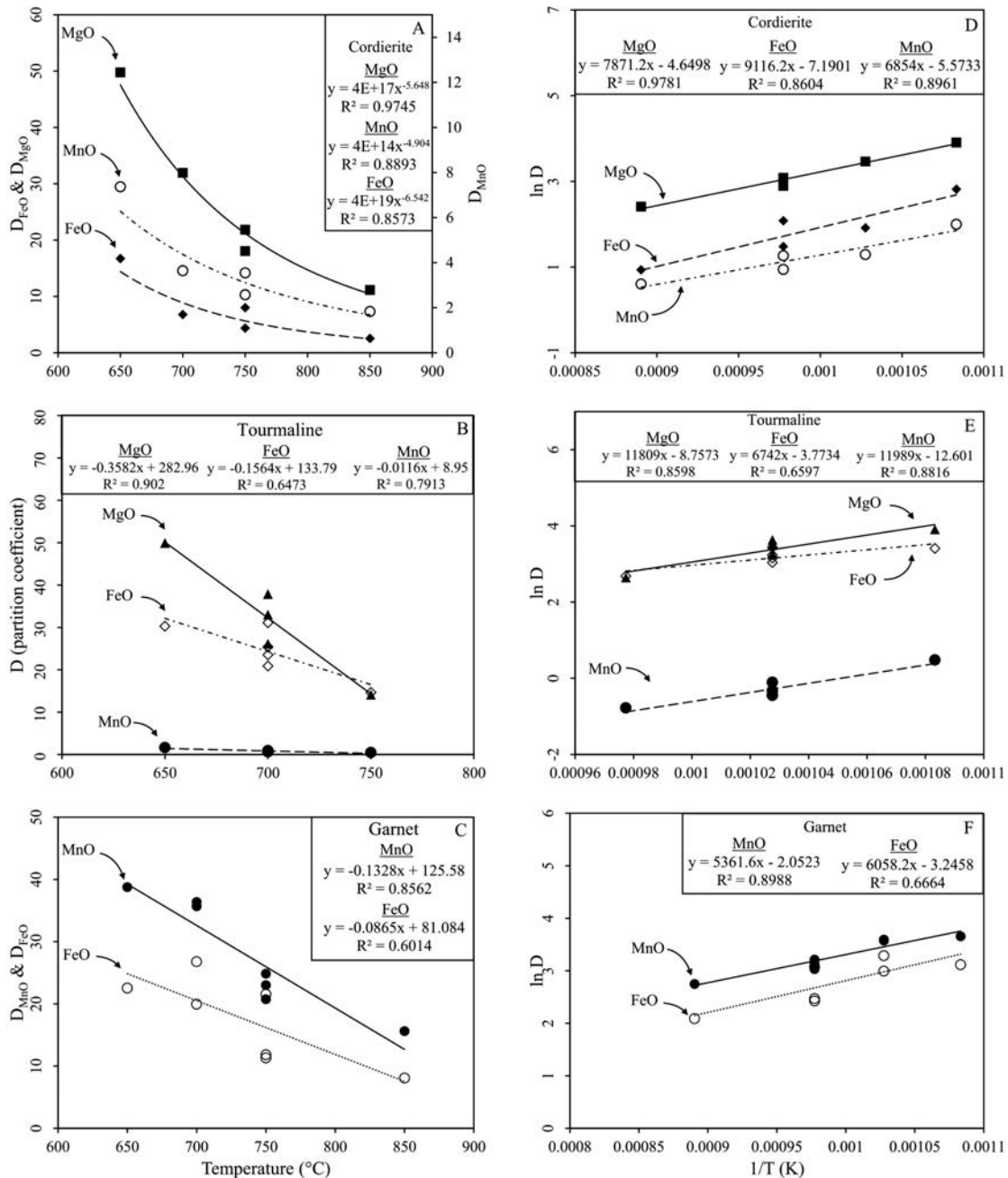


**FIGURE 6.** (a) Crd-melt partition coefficients,  $D_M$ , plotted against temperature. Individual points represent average values from individual experiments. (b) Tur-melt partition coefficients,  $D_M$ , plotted against temperature. Individual points represent average values of multiple experiments conducted at a given temperature. (c) Grt-melt partition coefficients,  $D_M$ , plotted against temperature. Individual points represent average values of multiple experiments conducted at a given temperature. (d–f) The partition coefficients presented in this study form a line when plotted in natural log D vs.  $1/T$  (K) space, which is supportive evidence of near-equilibrium conditions between crystals and melt.

ment GBT-103, Table 4) and biotite (Icenhower and London 1995) and a mode of 5 wt% for each individual mafic mineral, similar to modes of these minerals in natural occurrences. Initial ratios of MgO/FeO and MnO/FeO were calculated from the average composition of melt inclusions hosted by garnet in a metapelitic rock (Acosta-Vigil et al. 2007).

The vertical axis in Figures 8a and 8b represents values of

$C$ , the modeled MnO/FeO or MgO/FeO value of melt, and the horizontal axis is  $F$ , the fraction of liquid (melt) remaining. An increase in  $C$  reflects an increase in the MgO/FeO or MnO/FeO ratio of the residual melt, i.e., the exchange coefficient is less than one. The curves representing MgO/FeO and MnO/FeO in Figures 8a and 8b, respectively, show that crystallization of garnet will increase the MgO/FeO ratio and decrease the MnO/FeO of melt,

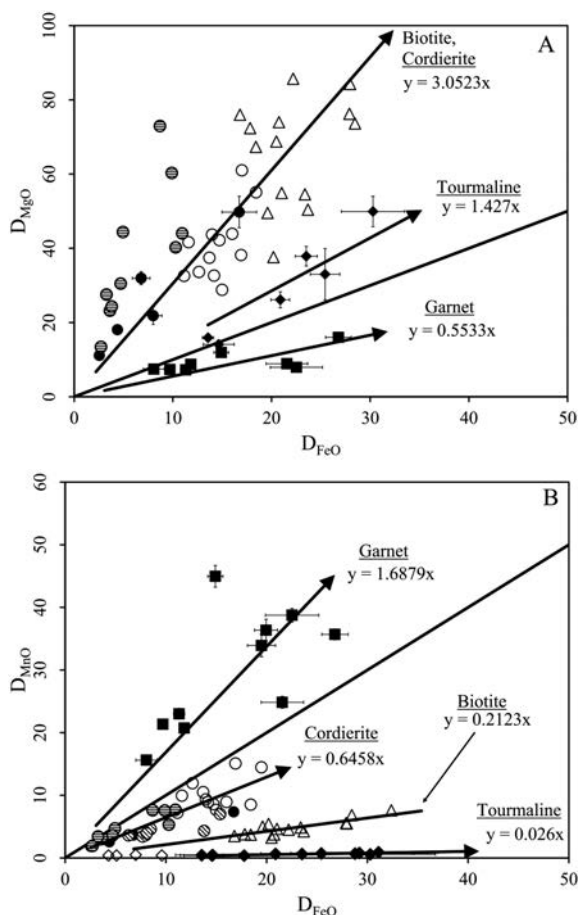


**FIGURE 7.** Mineral-melt exchange coefficients,  $K_D$ , calculated as the slope of a linear regression through the  $D_{FeO}$  and  $D_{MgO}$  data (a) and  $D_{MnO}$  and  $D_{FeO}$  data (b) for garnet-, tourmaline-, cordierite-, and biotite-melt. Solid symbols represent all data for garnet (squares), tourmaline (diamonds), and cordierite (circles) reported in the present manuscript. Open triangles, open circles, circles with horizontal lines, and circles with diagonal lines represent data from Icenhower and London (1995), Icenhower (1995), Evensen and London (2003), and Wolf and London (1997), respectively. The dashed black line without an arrow represents a one-to-one correlation of  $D_{FeO}$  and  $D_{MgO}$  (a) and  $D_{MnO}$  and  $D_{FeO}$  (b). The slope of each linear regression (solid black lines with arrows) represents an exchange coefficient for each mineral,  $K_{D(MgO/FeO)}$ . The exchange coefficients do not appear to depend on temperature considering data from experiments conducted in the temperature range of 850 to 650 °C. Individual data points represent average values calculated per individual experiment. Error bars show  $2\sigma$  standard deviations, which were propagated through the calculation of partition coefficients.

whereas crystallization of biotite, tourmaline, and cordierite has the opposite effect on melt composition.

Note that the modes of feldspar and quartz, or other non-mafic minerals, will not change the trends shown in Figures 8a and 8b due to much lower concentrations of Fe, Mn, and Mg in these non-mafic minerals. Also note that co-crystallization of two mafic minerals (e.g., cordierite and biotite) will produce a curve that lies in between the curves for the individual minerals. The absolute value of  $C$ , the ratio of MnO/FeO or MgO/FeO, depends on the

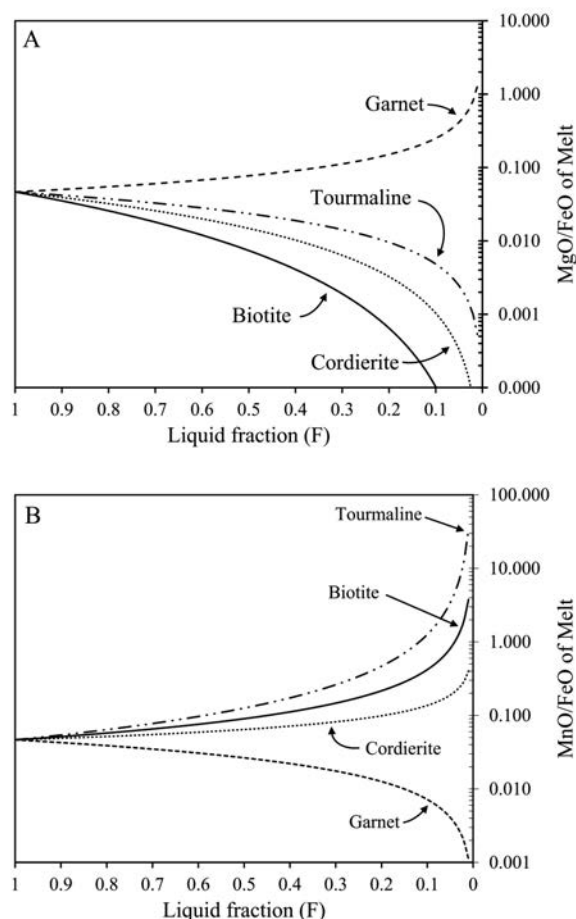


**FIGURE 8.** Rayleigh models for the evolution of the MgO/FeO (a) and MnO/FeO (b) ratios of granitic melt resulting from fractional crystallization of garnet, biotite, tourmaline, and cordierite individually at 650 °C and 200 MPa.  $F = 1$  represent 100% melt (liquid) and  $F = 0$  represents complete crystallization. The vertical axis represents values of  $C$  (MgO/FeO or MnO/FeO). Crystallization of garnet alone produces an increase in the MgO/FeO ratio and a decrease in the MnO/FeO ratio. Higher pressures (>400 MPa) may result in a different partitioning behavior.

temperature of crystallization, because the partition coefficients are temperature dependent (Fig. 6), the modes of mafic minerals, and the initial ratio of the concentrations of MnO and FeO. As a result, an increase in temperature will lead to a smaller change in the elemental ratios as fractional crystallization proceeds. The modes of mafic minerals used in Figures 8a and 8b are similar to natural occurrences and the initial ratios of elements (as oxides) were calculated from the composition of melt inclusions hosted by garnet in a metapelitic rock. The modeled ratios are similar to measured ratios of glass shards from garnet-saturated, rhyolitic ignimbrites (Caffè et al. 2012; Coira et al. 2018; Lucci et al. 2018).

#### Modeling the concentration of MnO during fractional crystallization

As a test of the  $D_M^{qtz}$  data reported in this manuscript, we use the garnet solubility data and  $D_M^{qtz}$  values (Figs. 4e and Table 4) in a Rayleigh model to evaluate the concentration of MnO during the fractional crystallization of an S-type granitic melt. The

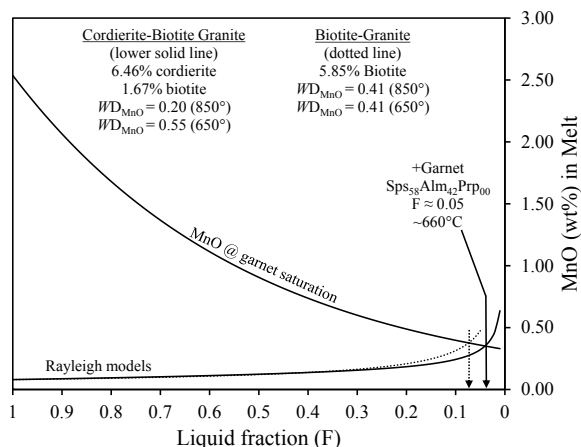


**FIGURE 9.** Rayleigh fractional crystallization model of an S-type granite liquid. The dashed line and the lower solid black line represent the results of two different Rayleigh models. The upper solid black line denotes the MnO saturation surface for garnet in B-bearing, hydrous granitic melt. The first model (solid black line) entails crystallization of a cordierite-biotite granite. The second model entails crystallization of a biotite granite (dashed line). Parameters for each Rayleigh model are reported in Supplemental<sup>2</sup> Material A. The models reveal that an anatectic S-type granitic magma must undergo 90% (biotite granite) to 95% (cordierite-biotite granite) crystallization before Mn-rich garnet will crystallize. Garnet-melt partition coefficients were varied as a function of temperature to calculate the composition of garnet that would crystallize from the modeled melt ( $D_{\text{MnO}} = 38.1$ ,  $D_{\text{FeO}} = 22.1$ ,  $D_{\text{MgO}} = 10.0$  at  $F = 0.05$ ).

model follows principles described by Janoušek et al. (2015). By design, the model pertains to the crystallization of a cordierite-bearing S-type granitic melt of anatectic origin that has migrated to pressures below ~400 MPa, such that almandine-pyrope solid solutions would likely not crystallize (Clemens and Wall 1981; Pereira and Bea 1994; Stevens et al. 2007). These results would apply to the cordierite-bearing granites of the Lachlan fold belt, Australia (White et al. 2001), similar granites in Western Europe (e.g., Strong and Hammer 1981; Bea et al. 1994; Villaseca and Barbero 1994; Villaseca et al. 1998), and leucogranites in the Himalayas (Nepal) (Visonà and Lombardo 2002).

The model begins with the average composition of 63 analyses of vitreous melt inclusions (MI) hosted by garnet in a quartz-absent, Grt-Bt-Sil metapelitic enclave within the El Hoyazo dacites, SE Spain, (Acosta-Vigil et al. 2007). Acosta-Vigil et al. (2010) concluded that the MIs in garnet were formed during the dehydration-melting of muscovite at a temperature of ~685–750 °C and pressure of 500–700 MPa. Though garnet is stable in the metapelitic enclave, at lower pressure (<400 MPa), cordierite (sekaninaite) will form at the expense of garnet (almandine) (Mukhopadhyay and Holdaway 1994) in a peraluminous liquid. Therefore, at 200 MPa and 800 °C, cordierite and biotite are stable mafic phases that could crystallize from the liquid represented by the MI in garnet. For comparison, a cordierite-free, biotite-granite is also modeled. Details regarding the calculation of mineral modes, bulk partition coefficients,  $WD$ , and how bulk partition coefficients were varied as a function of temperature ( $T$ ) and liquid fraction ( $F$ ) are presented in Tables S7 and S8 (Supplemental<sup>2</sup> Material A) and in Supplemental<sup>2</sup> Mate-

rial B. The partition coefficients for Mg, Fe, and Mn in quartz, plagioclase, and K-feldspar are set to zero. Therefore, their proportions on the liquid line of descent are irrelevant. Only their aggregate fraction matters to the evolution of melt composition with respect to mafic components. Note that the concentrations of all elements are used to calculate mineral modes and only the concentration of Mn is modeled using the Rayleigh equation.

The result of the Rayleigh model is depicted in Figure 9. In addition to the Rayleigh curve shown in Figure 9, the saturation surface for garnet in B-bearing, hydrous granitic melt, is also plotted, using the experimental data from this work in Figure 4e. The model representing the crystallization of the cordierite-bearing granite shows that the MnO content of melt intersects the saturation surface for garnet after ~95% fractional crystallization ( $F \approx 0.05$ ; ~660 °C, ~0.4 wt% MnO). The dashed curve in Figure 9 represents the result of the Rayleigh model for the crystallization of a cordierite-free biotite-granite. The dashed curve intersects the garnet saturation surface after ~90% crystallization. The composition of garnet that crystallizes in the models shown in Figure 9 ( $\text{Sps}_{58}\text{Alm}_{42}\text{Prp}_{00}$ ) was determined using the same garnet-melt partition coefficients used in the Rayleigh model ( $F = 0.04$ ,  $D_{\text{MnO}} = 38.1$ ,  $D_{\text{FeO}} = 22.1$ ,  $D_{\text{MgO}} = 10.0$ ). The results of the models shown in Figures 8a, 8b, and 9 are strikingly similar to the compositions of garnet and coexisting glass from Miocene-age, garnet-bearing rhyolitic ignimbrites in South America (Caffe et al. 2012; Coira et al. 2018; Lucci et al. 2018).

The  $D_{\text{MnO}}$  for cordierite-melt is noteworthy because it is greater than the  $D_{\text{MnO}}$  for biotite-melt, which means that cordierite-bearing S-type granites will require a greater extent of crystallization to reach saturation in Mn-rich garnet (Fig. 9), or may not achieve that saturation at all (e.g., Phillips et al. 1981; Pereira and Bea 1994; White et al. 2001). The paucity of garnet in the cordierite-bearing S-type granites of western Europe likely results from low-pressure fractional crystallization involving cordierite as the dominant ferromagnesian phase (e.g., Peña Negra complex, Avila batholith, Spain: Pereira and Bea 1994; Albuquerque pluton, Spain: London et al. 1999; Land's End pluton, U.K.: Müller et al. 2006).

Variations in melt composition and the choices of mafic minerals and their proportions will of course change the results shown in Figure 9 (see a discussion in Supplemental<sup>2</sup> Material B). Nonetheless, the Rayleigh model presented here using the partition coefficients of this study and partition coefficients reported in the literature produces a result with a hypothetical, but realistic, S-type granitic liquid that is consistent with natural occurrences of spessartine. To that extent, the agreement between the Rayleigh model and the natural occurrences leads to the conclusion that the partition coefficients derived from this study are applicable to natural settings. Moreover, partition coefficients for Mn between cordierite-melt (Evensen and London 2003), in which Mn is a trace to minor element, are similar to the values reported in this manuscript.

### Spessartine in granitic pegmatites

Spessartine is a common accessory mineral in LCT-type pegmatites (Laurs and Knox 2001). Rayleigh fractional crystallization, wherein the entire bulk melt remains in chemical equilibrium with the rims of growing crystals, is more applicable to the relatively

large masses of normal granite plutons than for granitic pegmatites, which are derived from the extended fractional crystallization of such plutons. The condition of equilibrium between crystals and a bulk melt whose composition changes continuously with crystallization does not apply to the internal evolution of granitic pegmatites (Morgan and London 1999; London et al. 2012b). Our partitioning data do show, however, that among the mafic minerals, the crystallization of tourmaline alone is the most effective driver of the melt composition to the high MnO/FeO ratios and MnO content that would foster the crystallization of spessartine. Tourmaline is a characteristic mineral of the border and wall zones of pegmatites (Cameron et al. 1949), where it tends to crystallize in abundance (e.g., Fig. 2 of Černý et al. 2012). As a result, spessartine, or Mn-phosphate equivalents (London and Burt 1982; London et al. 1999), are common phases in the interior zones of tourmaline-rich pegmatites.

### IMPLICATIONS

The experimentally derived mineral-melt partition coefficients,  $D_M^{O/L}$ , and exchange coefficients,  $K_{D(MN)}$ , presented in this study, confirm that the general fractionation trend of garnet in which the MnO/FeO ratio increases with increasing fractional crystallization (Černý et al. 1985) is controlled not by garnet itself but by other minerals that accommodate Fe and Mg over Mn. The data show that crystallization of garnet alone at the moderate pressures cited here will result in a decrease in the concentration of MnO in melt.

Among the minerals examined in this study, tourmaline is shown to be the most efficient at driving the concentration of MnO in melt to garnet saturation. Although Mn behaves compatibly in cordierite and biotite, Fe and Mg are so much more compatible that the MnO content of melt increases when biotite or even cordierite dominates the mafic mineral assemblage. However, granites that contain mostly cordierite may never reach garnet saturation.

This study elucidates part of the geochemical cycle of Mn in the continental crust: the accommodation and enrichment of Mn in granitic liquids from deep sources of anatexis to shallow levels of solidification and crystallization of spessartine-bearing granites and pegmatites. These results bear directly on the formation of highly prized, gem-quality spessartine, which is mined from granitic pegmatites (Lauris and Knox 2001). The measured partition coefficients may also be pertinent to other types of Mn ores (e.g., Roy 1997).

The model presented here indicates that extensive fractional crystallization ( $\geq 90\%$ ) of a starting anatectic melt is necessary to bring granitic liquids to saturation in spessartine at near-solidus conditions. Likewise, beryl (Be), tourmaline (B), spodumene (Li), and pollucite (Cs) achieve saturation in pegmatite-forming melts only after very extended fractional crystallization, and mostly at subsolidus temperatures of crystallization (i.e., in highly undercooled melt: London 2008). This study adds one more piece of evidence to the paradigm for rare-element pegmatites: such bodies arise only from extended fractionated of large granitic bodies and cannot arise directly from small batches of anatectic melts (cf. Stewart 1978; Shearer et al. 1992; Simmons et al. 1996).

### ACKNOWLEDGMENTS

We thank George B. Morgan VI for leading the first author through the development of electron microbeam methods, useful discussions on the design, documentation, interpretation of experiments, and for editorial revisions on several drafts of the

manuscript. Thanks go to Calvin Miller, Victoria Maneta, and two anonymous reviewers for their thoughtful and constructive reviews and to Associate Editor Don Baker for handling of the manuscript.

### FUNDING

This study was funded in part by NSF grants EAR-0946322 and EAR-1623110 to D.L. The electron microprobe laboratory at OU was created by DOE grant DE-FG22-87FE1146, with upgrades from NSF EAR-8720498, EAR-9404658, EAR-0649001, and EAR-1401940, and continuing support from the Vice President of Research at OU.

### REFERENCES CITED

- Acosta-Vigil, A., London, D., Morgan, G.B. IV, and Dewers, T.A. (2003) Solubility of excess alumina in hydrous granitic melts in equilibrium with peraluminous minerals at 700–800°C and 200 MPa, and applications of the aluminum saturation index. *Contributions to Mineralogy and Petrology*, 146, 100–119.
- Acosta-Vigil, A., Cesare, B., London, D., and Morgan, G.B. (2007) Microstructures and composition of melt inclusions in a crustal anatectic environment, represented by metapelitic enclaves within El Hoyazo dacites, SE Spain. *Chemical Geology*, 237, 450–465.
- Acosta-Vigil, A., Buick, I.S., Hermann, J., Cesare, B., Rubatto, D., London, D., and Morgan, G.B. (2010) Mechanisms of crustal anatexis: a geochemical study of partially melted metapelitic enclaves and host dacite, SE Spain. *Journal of Petrology*, 51, 785–821.
- Baker, L.R., and Rutherford, M.J. (1996) The effect of dissolved water on the oxidation state of silicic melts. *Geochimica et Cosmochimica Acta*, 60, 2179–2187.
- Bea, F. (1996) Controls on the trace element composition of crustal melts. In M. Brown, P.A. Candela, D.L. Peck, W.E. Stephens, R.J. Walker, and E.-A. Zen, Eds., *The third Hutton symposium on the origin of granites and related rocks*, pp. 33–41. Geological Society of America Special Paper.
- Bea, F., Pereira, M.D., Corretge, L.G., and Fershtater, G.B. (1994) Differentiation of strongly peraluminous, perphosphorous granites: The Pedrobernardo pluton, central Spain. *Geochimica et Cosmochimica Acta*, 58, 2609–2627.
- Beattie, P., Drake, M., Jones, J., Leeman, W., Longhi, J., McKay, G., Nielsen, R., Palme, H., Shaw, D., Takahashi, E., and others. (1993) Terminology for trace-element partitioning. *Geochimica et Cosmochimica Acta*, 57, 1605–1606.
- Berndt, J., Koepke, J., and Holtz, F. (2005) An experimental investigation of the influence of water and oxygen fugacity on differentiation of MORB at 200 MPa. *Journal of Petrology*, 46, 135–167.
- Caffe, P.J., Trumbull, R.B., and Siebel, W. (2012) Petrology of the Coyaguayma ignimbrite, northern Puna of Argentina: Origin and evolution of a peraluminous high-SiO<sub>2</sub> rhyolite magma. *Lithos*, 134–135, 179–200.
- Cameron, E.N., Jahns, R.H., McNair, A.H., and Page, L.R. (1949) Internal structure of granitic pegmatites. *Economic Geology Monograph* 2.
- Černý, P., Meintzer, R.E., and Anderson, A.J. (1985) Extreme fractionation in rare-element granitic pegmatites: Selected examples of data and mechanisms. *Canadian Mineralogist*, 23, 381–421.
- Černý, P., Chapman, R., Schreyer, W., Ottolini, L., Bottazzi, P., and McCammon, C.A. (1997) Lithium in sekaninaite from the type locality, Dolní Bory, Czech Republic. *Canadian Mineralogist*, 35, 167–173.
- Černý, P., London, D., and Novák, M. (2012) Granitic pegmatites as reflections of their sources. *Elements*, 8, 289–294.
- Chappell, B.W., and White, A.J.R. (2001) Two contrasting granite types: 25 years later. *Australian Journal of Earth Sciences*, 48, 489–499.
- Christiansen, E.H., Bikun, J.V., Sheridan, M.F., and Burt, D.M. (1984) Geochemical evolution of topaz rhyolites from the Thomas Range and Spor Mountain, Utah. *American Mineralogist*, 69, 223–236.
- Clemens, J.D., and Wall, V.J. (1981) Origin and crystallization of some peraluminous (S-type) granitic magmas. *Canadian Mineralogist*, 19, 111–131.
- Coira, B., Kay, S.M., Viramonte, J.G., Kay, R.W., and Galli, C. (2018) Origin of late Miocene peraluminous Mn-rich garnet-bearing rhyolitic ashes in the Andean Foreland (Northern Argentina). *Journal of Volcanology and Geothermal Research*.
- Dasgupta, H.C., Seifert, F., and Schreyer, W. (1974) Stability of manganocordierite and related phase equilibria in part of the system MnO-Al<sub>2</sub>O<sub>3</sub>-SiO<sub>2</sub>-H<sub>2</sub>O. *Contributions to Mineralogy and Petrology*, 43, 275–294.
- Dwivedi, S.B., Mohan, A., and Lal, R.K. (1998) Recalibration of the Fe-Mg exchange reaction between garnet and cordierite as a thermometer. *European Journal of Mineralogy*, 10, 281–289.
- Evensen, J.M., and London, D. (2003) Experimental partitioning of Be, Cs, and other trace elements between cordierite and felsic melt, and the chemical signature of S-type granite. *Contributions to Mineralogy and Petrology*, 144, 739–757.
- Ewart, A., and Griffin, W.L. (1994) Application of proton-microprobe data to trace-element partitioning in volcanic rocks. *Chemical Geology*, 117, 251–284.
- Frost, B.R., Barnes, C.G., Collins, W.J., Arculus, R.J., Ellis, D.J., and Frost, C.D. (2001) A geochemical classification for granitic rocks. *Journal of Petrology*, 42, 2033–2048.
- Grew, E.S., Locock, A.J., Mills, S.J., Galuskin, I.O., Galuskin, E.V., and Hälenius, U. (2013) IMA report: Nomenclature of the garnet supergroup. *American Mineralogist*, 98, 785–811.
- Henry, D.J., Novák, M., Hawthorne, F.C., Ertl, A., Dutrow, B.L., Uher, P., and Pez-

- zotta, F. (2011) Nomenclature of the tourmaline-supergroup minerals. *American Mineralogist*, 96, 895–913.
- Higuchi, H., and Nagasawa, H. (1969) Partition of trace elements between rock-forming minerals and the host volcanic rocks. *Earth and Planetary Science Letters*, 7, 281–287.
- Holdaway, M.J. (2004) Optimization of some key geothermobarometers for pelitic metamorphic rocks. *Mineralogical Magazine*, 68, 1–14.
- Huebner, J.S., and Sato, M. (1970) The oxygen fugacity-temperature relationships of manganese oxide and nickel oxide buffers. *American Mineralogist*, 55, 934–952.
- Icenhower, J.P. (1995) Experimental determination of element behavior in silicic systems during hydrous partial fusion. University of Oklahoma, Norman, U.S.A.
- Icenhower, J.P., and London, D. (1995) An experimental study of element partitioning among biotite, muscovite, and coexisting peraluminous silicic melt at 200 MPa (H<sub>2</sub>O). *American Mineralogist*, 80, 1229–1251.
- Janoušek, V., Moya, J.F., Martín, H., Erban, V., and Farrow, C. (2015) Geochemical Modelling of Igneous Processes—Principles and Recipes in R Language: Bringing the power of R to a geochemical community. Springer-Verlag.
- Jobin-Bevans, S., and Černý, P. (1998) The beryllian cordierite + beryl + spessartine assemblage, and secondary beryl in altered cordierite, Greer Lake Granitic Pegmatites, Southeastern Manitoba. *Canadian Mineralogist*, 36, 447–462.
- Laurs, B.M., and Knox, K. (2001) Spessartine garnet from Ramona, San Diego County, California. *Gems & Gemology*, 37, 278–295.
- London, D. (2008) Pegmatites. Special publication, *Canadian Mineralogist*, vol. 10, 347 p.
- London, D., and Burt, D.M. (1982) Alteration of spodumene, montebasite and lithophilite in pegmatites of the White Picacho district, Arizona. *American Mineralogist*, 67, 97–113.
- London, D., Wolf, M.B., Morgan, G.B. VI, and Garrido, M.G. (1999) Experimental silicate–phosphate equilibria in peraluminous granitic magmas, with a case study of the Alburquerque Batholith at Tres Arroyos, Badajoz, Spain. *Journal of Petrology*, 40, 215–240.
- London, D., Evensen, J.M., Fritz, E.A., Icenhower, J.P., Morgan, G.B., and Wolf, M.B. (2001) Enrichment and accommodation of manganese in granite-pegmatite systems. In Eleventh Annual V.M. Goldschmidt Conference p. abstract no. 3369. Hot Springs, Virginia.
- London, D., Morgan, G.B., and Acosta-Vigil, A. (2012a) Experimental simulations of anatexis and assimilation involving metapelite and granitic melt. *Lithos*, 153, 292–307.
- London, D., Morgan, G.B., Paul, K.A., and Guttry, B.M. (2012b) Internal evolution of miarolitic granitic pegmatites at the little three Mine, Ramona, California, USA. *Canadian Mineralogist*, 50, 1025–1054.
- Lucci, F., Rossetti, F., Becchio, R., Theye, T., Gerdes, A., Opitz, J., Baez, W., Bardelli, L., De Astis, G., Viramonte, J., and others. (2018) Magmatic Mn-rich garnets in volcanic settings: Age and longevity of the magmatic plumbing system of the Miocene Ramadas volcanism (NW Argentina). *Lithos*.
- Mahood, G.A., and Hildreth, E.W. (1983) Large partition coefficients for trace elements in high-silica rhyolites. *Geochimica et Cosmochimica Acta*, 47, 11–30.
- Maner, J.L., London, D., and Morgan, G.B. (2013) Toward an experimentally calibrated garnet-tourmaline geothermometer. In Geological Society of America Abstracts with Programs p. 17. Austin, Texas.
- (2014) Elemental partitioning and zoning in tourmaline: An experimental investigation. In Goldschmidt Conference Abstracts. Sacramento, California.
- Matsui, Y., Onuma, N., Nagasawa, H., Higuchi, H., and Banno, S. (1977) Crystal structure control in trace element partition between crystal and magma. *Tectonics*, 100, 315–324.
- Miller, C.F., and Stoddard, E.F. (1981) The role of manganese in the paragenesis of magmatic garnet: An example from the Old Woman-Piute Range, California. *The Journal of Geology*, 89, 233–246.
- Moore, G., Righter, K., and Carmichael, I.S.E. (1995) The effect of dissolved water on the oxidation state of iron in natural silicate liquids. *Contributions to Mineralogy and Petrology*, 120.
- Morgan, G.B. (2016) A spreadsheet for calculating normative mole fractions of end-member species for Na-Ca-Li-Fe<sup>2+</sup>-Mg-Al tourmalines from electron microprobe data. *American Mineralogist*, 101, 111–119.
- Morgan, G.B., and London, D. (1996) Optimizing the electron microprobe analysis of hydrous alkali aluminosilicate glasses. *American Mineralogist*, 81, 1176–1185.
- (1999) Crystallization of the Little Three layered pegmatite-aplite dike, Ramona District, California. *Contributions to Mineralogy and Petrology*, 136, 310–330.
- (2005) Effect of current density on the electron microprobe analysis of alkali aluminosilicate glasses. *American Mineralogist*, 90, 1131–1138.
- Mukhopadhyay, B., and Holdaway, M.J. (1994) Cordierite-garnet-sillimanite-quartz equilibrium: I. New experimental calibration in the system FeO-Al<sub>2</sub>O<sub>3</sub>-SiO<sub>2</sub>-H<sub>2</sub>O and certain P-T-X<sub>H<sub>2</sub>O</sub> relations. *Contributions to Mineralogy and Petrology*, 116, 462–472.
- Müller, A., Seltmann, R., Halls, C., Siebel, W., Dulski, P., Jeffries, T., Spratt, J., and Kronz, A. (2006) The magmatic evolution of the Land's End Pluton, Cornwall, and associated pre-enrichment of metals. *Ore Geology Reviews*, 28, 329–367.
- Müller, A., Kearsley, A., Spratt, J., and Seltmann, R. (2012) Petrogenetic implications of magmatic garnet in granitic pegmatites from Southern Norway. *Canadian Mineralogist*, 50, 1095–1115.
- Nash, W.P., and Crecraft, H.R. (1985) Partition coefficients for trace elements in silicic magmas. *Geochimica et Cosmochimica Acta*, 49, 309–322.
- Pereira, M.D., and Bea, F. (1994) Cordierite-producing reactions in the Pena Negra complex, Avila batholith, central Spain: The key role of cordierite in low-pressure anatexis. *Canadian Mineralogist*, 31, 763–780.
- Phillips, G.N., Wall, V.J., and Clemens, J.D. (1981) Petrology of the Strathgogie batholith: a cordierite-bearing granite. *Canadian Mineralogist*, 19, 47–63.
- Pouchou, J.L., and Pichoir, F. (1985) "PAP" (ρ-p-ρ) correction procedure for improved quantitative microanalysis. In *Microbeam Analysis* pp. 104–106. San Francisco Press, California.
- Puziewicz, J., and Johannes, W. (1988) Phase equilibria and compositions of Fe-Mg-Al minerals and melt in water saturated peraluminous granitic systems. *Contributions to Mineralogy and Petrology*, 100, 156–168.
- Roeder, P.L., and Emslie, R.F. (1970) Olivine-liquid equilibrium. *Contributions to Mineralogy and Petrology*, 29, 275–289.
- Romer, R.L., Kirsch, M., and Kroner, U. (2011) Geochemical signature of Ordovician Mn-rich sedimentary rocks on the Avalonian shelf. *Canadian Journal of Earth Sciences*, 48, 703–718.
- Roy, S. (1997) Genetic diversity of manganese deposition in the terrestrial geological record, Special Publication, 5–27 p. Geological Society, London.
- Shearer, C.K., Papike, J.J., and Jolliff, B.L. (1992) Petrogenetic links among granites and pegmatites in the Harney Peak rare-element granite-pegmatite system, Black Hills, South Dakota. *Canadian Mineralogist*, 30, 785–809.
- Simmons, W.B., Foord, E.E., Falster, A.U., and King, V.T. (1996) Evidence for an anatectic origin of granitic pegmatites, western Maine, USA. In Geological Society of America Abstracts with Programs p. 27, 411.
- Stevens, G., Villaros, A., and Moya, J.F. (2007) Selective peritectic garnet entrapment as the origin of geochemical diversity in S-type granites. *Geology*, 35, 9–12.
- Stewart, D.B. (1978) Petrogenesis of lithium-rich pegmatites. *American Mineralogist*, 63, 970–980.
- Strong, D.F., and Hammer, S.K. (1981) The leucogranites of southern Brittany: origin by faulting, frictional heating, fluid flux and fractional melting. *Canadian Mineralogist*, 19, 163–176.
- Taylor, J.F., and Wall, V.J. (1992) The behavior of tin in granitoid magmas. *Economic Geology*, 87, 403–420.
- Ulmer, P. (1989) The dependence of the Fe<sup>2+</sup>-Mg cation-partitioning between olivine and basaltic liquid on pressure, temperature, and composition—An experimental study to 30 kbars. *Contributions to Mineralogy and Petrology*, 101, 261–273.
- van Hinsberg, V.J. (2011) Preliminary experimental data on trace-element partitioning between tourmaline and silicate melt. *Canadian Mineralogist*, 49, 153–163.
- van Hinsberg, V.J., and Schumacher, J.C. (2009) The geothermobarometric potential of tourmaline, based on experimental and natural data. *American Mineralogist*, 94, 761–770.
- Villaseca, C., and Barbero, L. (1994) Chemical variability of Al-Ti-Fe-Mg minerals in peraluminous granitoid rocks from Central Spain. *European Journal of Mineralogy*, 6, 691–710.
- Villaseca, C., Barbero, L., and Rogers, G. (1998) Crustal origin of Hercynian peraluminous granitic batholiths of Central Spain: petrological, geochemical and isotopes (Sr, Nd) constraints. *Lithos*, 43, 55–79.
- Visonà, D., and Lombardo, B. (2002) Two-mica and tourmaline leucogranites from the Everest-Makalu region (Nepal-Tibet). Himalayan leucogranite genesis by isobaric heating? *Lithos*.
- White, A.J.R., Allen, C.M., Beams, S.D., Carr, P.F., Champion, D.C., Chappell, B.W., Wyborn, D., and Wyborn, L.A.I. (2001) Granite suites and supersuites of Eastern Australia. *Australian Journal of Earth Sciences*, 48, 515–530.
- Whitney, D.L., and Evans, B.W. (2010) Abbreviations for names of rock-forming minerals. *American Mineralogist*, 95, 185–187.
- Wolf, M.B., and London, D. (1997) Boron in granitic magmas: stability of tourmaline in equilibrium with biotite and cordierite. *Contributions to Mineralogy and Petrology*, 130, 12–30.
- Wolf, M.B., London, D., and Morgan, G.B. (1994) Effects of boron on the solubility of cassiterite and tantalite in granitic liquids. In Geological Society of America Abstracts with Programs.

MANUSCRIPT RECEIVED DECEMBER 21, 2018

MANUSCRIPT ACCEPTED JULY 27, 2019

MANUSCRIPT HANDLED BY DON BAKER

## Endnotes:

- <sup>1</sup>Mineral-melt exchange coefficients are equivalent to Nernst distribution coefficients, which represent the product of a homogeneous exchange reaction. In this case, the reaction is between crystal and melt. Crystallization of minerals from melt represents the principal and only feasible means of measuring the elemental partition coefficients. A reversal of this reaction requires diffusion of the element(s) of interest out of a crystal into melt until both phases, crystal and melt, have been equilibrated. Solid-state diffusion of mafic components through a crystalline phase is impossibly slow on the time frames of experiments. Moreover, a crystal that is not in equilibrium with melt will dissolve at a rate much greater than that of the solid-state diffusion of ions through the crystal (e.g., Bea 1996).
- <sup>2</sup>Deposit item AM-19-116938, Supplemental Material. Deposit items are free to all readers and found on the MSA website, via the specific issue's Table of Contents (go to [http://www.minsocam.org/MSA/AmMin/TOC/2019/Nov2019\\_data/Nov2019\\_data.html](http://www.minsocam.org/MSA/AmMin/TOC/2019/Nov2019_data/Nov2019_data.html)).